 CMES, vol.4, no.2, pp.259-271, 2003

A Buckling and Postbuckling Analysis of Rods Under End Torque and Compressive Load

Wen Yi Lin[1] **and Kuo Mo Hsiao**[2]

Abstract: The buckling and postbuckling behavior of spatial rods under different types of end torque and compressive axial force is investigated using finite element method. All coupling among bending, twisting, and stretching deformations for beam element is considered by consistent second-order linearization of the fully geometrically nonlinear beam theory. However, the third order term of the twist rate is also considered. An incremental-iterative method based on the Newton-Raphson method combined with constant arc length of incremental displacement vector is employed for the solution of nonlinear equilibrium equations. The zero value of the tangent stiffness matrix determinant of the structure is used as the criterion of the buckling state. Numerical examples are presented to investigate the effect of aspect ratio of the rectangular cross section and compressive force on the buckling torque and postbuckling behavior of spatial rods under different types of end torque.

keyword: Torsion, Buckling, Postbuckling, Beam, Geometrical nonlinearity.

1 Introduction

A rod under the action of torque may exhibit a buckling behavior [Brush and Almroth (1975)]. The nature of a torque depends on the mechanism that generates the torque. Different ways for generating configuration dependent torque were proposed in the literature [Ziegler (1977); Argyris, Dunne, and Scharpf (1978); Iura and Atluri (1988); Teh and Clarke (1997); Hsiao, Yang and Lin (1998)]. The buckling analysis of spatial rods under end torques was first studied by Greenhill (1883), and followed by [Ziegler (1952); Beck (1955); Yang and Kuo (1991); Goto, Li, and Kasugal (1996)]. Except [Goto, Li, and Kasugal (1996)], all of these researches are linear buckling analysis. A limitation of the linear buckling analysis has been the omission of any consideration of the effect of prebuckling deflections of the beam. In many cases, however, the effect of the prebuckling deflections must be taken into account if the buckling load is to be determined with accuracy [Brush and Almroth (1975)]. Moreover, the linear buckling analysis gives no information about the shape of the secondary path. Sometimes the behavior of a structure can be understood only if the shape of the secondary path is known. In [Goto, Li, and Kasugal (1996)], the prebuckling torsional deformation was considered for the buckling analysis of spatial rods under end torsional moment. The rods considered are clamped at one end and are free to translate along the axis of the rod and rotate about the axis of the rod at another end. Numerical results for rods with rectangular cross section were given in [Goto, Li, and Kasugal (1996)]. It was observed that except the rod with square cross section, the discrepancy between the buckling moments corresponding to the linear buckling analysis and the nonlinear buckling analysis was remarked. However, the axial deformation due to twist, which is proportional to the square of the twist rate, was not considered in [Goto, Li, and Kasugal (1996)]. Timoshenko (1956) mentioned that owing to this axial deformation, there is an additional resistance of the shaft to torsion proportional to the cube of the twist rate. In the case of a very narrow rectangular cross section and comparatively large twist rate, the additional resistance corresponding to the cube of the twist rate may contribute an important portion of the total torque [Timoshenko (1956); Gregory (1960); Hsiao and Lin (2000)]. Moreover, due to the rotational boundary conditions used in [Goto, Li, and Kasugal (1996)], the ways of generating end moment are rendered irrelevant. When the rods are clamped at one end and free at another end, the buckling and postbuckling behavior of rods under different types of end torque may be different. However, little information in the literature is available, especially when the axial compressive

[1] Department of Mechanical Engineering, De Lin Institute of Technology, Tucheng, Taiwan.
[2] Department of Mechanical Engineering , National Chiao Tung University, Hsinchu , Taiwan

load is also considered.

The objective of the present paper is to investigate the buckling and postbuckling behavior of rods under different types of end torque and the axial force using finite element method. Many different finite formulations and numerical procedures for the buckling and postbuckling analysis of three-dimensional beams have been proposed [Argyris, Dunne, and Scharpf (1978); Attard (1986); Simo and Vu-Quoc (1986); Crisfield (1990); Izzuddin and Smith (1996); Teh and Clarke (1998); Hsiao, and Lin (2000); Atluri, Iura and Vasudevan (2001); Ijima K., Obiya H., Iguchi S., and Goto S. (2003)]. In general, the zero value of the tangent stiffness matrix determinant of the structure is used as the criterion of the buckling state. However, not all the tangent stiffness matrices given in the literature can be used in detecting buckling state of rods under different types of end torque and the axial force. Hsiao and Lin (2000) presented a consistent co-rotational total Lagrangian finite element formulation for the geometrical nonlinear analysis of three-dimensional elastic Euler beam. All coupling among bending, twisting, and stretching deformations for beam element was considered by consistent second-order linearization of the fully geometrically nonlinear beam theory. However, the third order term of the twist rate of the beam axis is also considered in the element nodal forces. The method is proven very effective for geometrical nonlinear analysis of three-dimensional elastic Euler beam by numerical examples studied by [Hsiao and Lin (2000)]. Thus, the formulation of beam element proposed in [Hsiao and Lin (2000)] is employed in this study.

An incremental-iterative method based on the Newton-Raphson method combined with constant arc length of incremental displacement vector is employed for the solution of nonlinear equilibrium equations. The zero value of the tangent stiffness matrix determinant of the structure is used as the criterion of the buckling state. Numerical examples are presented to investigate the effect of aspect ratio of the rectangular cross section and compressive force on the buckling torque and postbuckling behavior of spatial rods under different types of end torque.

2 Finite element formulation

In the following only a brief description of the beam element is given. The more detailed description may be obtained from [Hsiao (1992); Hsiao and Lin (2000)].

2.1 Basic assumptions

The following assumptions are made in derivation of the beam element behavior.

1. The beam is doubly symmetric, uniform and slender, and the Euler-Bernoulli hypothesis is valid.
2. The unit extension and the twist rate of the centroid axis of the beam element are uniform.
3. The cross section of the beam element does not deform in its own plane and strains within this cross section can be neglected.

A beam of monosymmetric or unsymmetric sections, except that of Z-section, subjected to pure torque generates not only twisting but also bending in two principal planes [Gregory (1960)]. Thus only the beam of doubly symmetric sections is considered here.

2.2 Coordinate systems

In this paper, a co-rotational total Lagrangian formulation is adopted. In order to describe the system, we define four sets of right handed rectangular Cartesian coordinate systems:

1. A fixed global set of coordinates, X_i^G (i = 1, 2, 3) (see Fig. 1); the nodal coordinates, displacements, and rotations, and the stiffness matrix of the system are defined in this coordinates.
2. Element cross section coordinates, x_i^S (i = 1, 2, 3) (see Fig. 1); a set of element cross section coordinates is associated with each cross section of the beam element. The origin of this coordinate system is rigidly tied to the centroid of the cross section. The x_1^S axes are chosen to coincide with the normal of the unwarpped cross section and the x_2^S and x_3^S axes are chosen to be the principal directions of the cross section.
3. Element coordinates; x_i (i = 1, 2, 3) (see Fig. 1), a set of element coordinates is associated with each element, which is constructed at the current configuration of the beam element. The origin of this coordinate system is located at node 1. The x_1 axis is chosen to pass through two end nodes of the element; the x_2 and x_3 axes are chosen to be the principal directions of the cross section at the undeformed

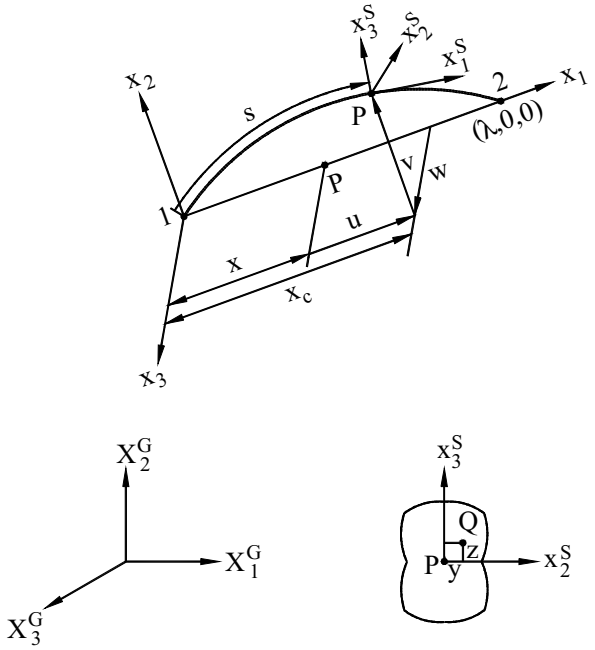

Figure 1 : Coordinate systems

state. The deformations, internal nodal forces and stiffness matrix of the elements are defined in terms of these coordinates.

4. Load base coordinates, X_i^P (i = 1, 2, 3); a set of load base coordinates is associated with each configuration dependent moment. The origin of this coordinate system is chosen to be the node where the configuration dependent moment is applied. The mechanism for generating configuration dependent moment is described in these coordinates.

2.3 Rotation vector

For convenience of the later discussion, the term 'rotation vector' is used to represent a finite rotation. Figure 2 shows that a vector **b**, which as a result of the application of a rotation vector $\phi\mathbf{a}$ is transported to the new position $\overline{\mathbf{b}}$. The relation between $\overline{\mathbf{b}}$ and **b** may be expressed as [Goldstein (1980)]

$$\overline{\mathbf{b}} = \cos\phi\mathbf{b} + (1-\cos\phi)(\mathbf{a}\cdot\mathbf{b})\mathbf{a} + \sin\phi(\mathbf{a}\times\mathbf{b}) \tag{1}$$

where ϕ is the angle of rotation about the axis of rotation, and **a** is the unit vector along the axis of rotation.

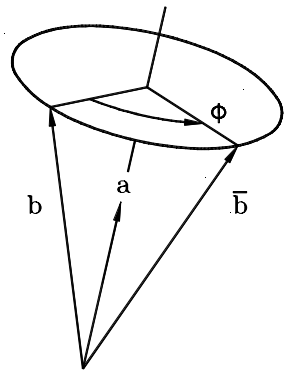

Figure 2 : Rotation vector.

2.4 Kinematics of beam element

The deformations of the beam element are described in the current element coordinate system. Let Q (Fig. 1) be an arbitrary point in the beam element, and P be the point corresponding to Q on the shear center axis. The position vector of point Q in the undeformed and deformed configurations may be expressed as

$$\mathbf{r}_0 = x\mathbf{e}_1 + y\mathbf{e}_2 + z\mathbf{e}_3, \tag{2}$$

$$\begin{aligned}\mathbf{r} = {} & x_c(x)\mathbf{e}_1 + v(x)\mathbf{e}_2 + w(x)\mathbf{e}_3 \\ & + \theta_{1,x}\omega(y,z)\mathbf{e}_1^S + y\mathbf{e}_2^S + z\mathbf{e}_3^S \ ,\end{aligned} \tag{3}$$

where $x_c(x)$, $v(x)$,and $w(x)$ are the x_1, x_2 and x_3 coordinates of point P, respectively, in the deformed configuration, $\theta_{1,x}$ is the twist rate of the shear center axis, $\omega(y,z)$ is the Saint Venant warping function for a prismatic beam of the same cross section, and $\mathbf{e}_i$ and $\mathbf{e}_i^S$ (i = 1, 2, 3) denote the unit vectors associated with the x_i and x_i^S axes, respectively. Note that $\mathbf{e}_i$ and $\mathbf{e}_i^S$are coincident in the undeformed state. Here, the triad $\mathbf{e}_i^S$ in the deformed state is assumed to be achieved by the successive application of the following two rotation vectors to the triad $\mathbf{e}_i$:

$$\boldsymbol{\theta}_n = \theta_n\{0,\ \theta_2/(\theta_2^2+\theta_3^2)^{1/2},\ \theta_3/(\theta_2^2+\theta_3^2)^{1/2}\} = \theta_n\mathbf{n} \tag{4}$$

$$\boldsymbol{\theta}_t = \theta_1\{(1-\theta_2^2-\theta_3^2)^{1/2},\ \theta_3,\ -\theta_2\} = \theta_1\mathbf{t} \tag{5}$$

where

$$\theta_2 = -\frac{dw(x)}{ds} = -\frac{dw(x)}{dx}\frac{dx}{ds} = -\frac{w'}{1+\varepsilon_c},$$

$$\theta_3 = \frac{dv(x)}{ds} = \frac{dv(x)}{dx}\frac{dx}{ds} = \frac{v'}{1+\varepsilon_c} \tag{6}$$

$$\varepsilon_c = \frac{\partial s}{\partial x} - 1 \tag{7}$$

in which $\mathbf{n}$ is the unit vector perpendicular to the vectors $\mathbf{e}_1$ and $\mathbf{e}_1^S$, and $\mathbf{t}$ is the tangent unit vector of the deformed shear center axis of the beam element. $\theta_1$is the rotation about vector $\mathbf{t}\cdot\theta_n$ is the angle measured from x_1 axis to vector $\mathbf{t}$, ε_c is the unit extension of the shear center axis and s is the arc length of the deformed shear center axis measured from node 1 to point P.

Using Eqs 1-5, the relation between the vectors $\mathbf{e}_i$ and $\mathbf{e}_i^S$ (i = 1, 2, 3) in the element coordinate system may be obtained as [Hsiao (1992)]

$$\mathbf{e}_i^S = \mathbf{R}\mathbf{e}_i \tag{8}$$

where $\mathbf{R}$ is the so-called rotation matrix. The rotation matrix is determined byθ_i (i = 1, 2, 3). Thus, θ_i are called rotation parameters in this study.

The relationship among $x_c(x)$, $v(x)$, $w(x)$, and s may be given as

$$x_c(x) = u_1 + \int_0^x [(1+\varepsilon_c)^2 - v_{,x}^2 - w_{,x}^2]^{1/2} dx \tag{9}$$

where u_1 is the displacement of node 1 in the x_1 direction. Note that due to the definition of the element coordinate system, the value of u_1 is equal to zero.

Here, the lateral deflections of the shear center axis, $v(x)$ and $w(x)$ are assumed to be the cubic Hermitian polynomials of x, and the rotation about the shear center axis $\theta_1(x)$ (Eq. 5) is assumed to be the linear polynomials of x. $v(x)$, $w(x)$ and $\theta_1(x)$ may be expressed by

$$v(x) = \mathbf{N}_b^t \mathbf{u}_b,\ \ w(x) = \mathbf{N}_c^t \mathbf{u}_c,\ \ \theta_1(x) = \mathbf{N}_d^t \mathbf{u}_d \tag{10}$$

$$\mathbf{u}_b = \left\{v_1, v_1', v_2, v_2'\right\}, \quad \mathbf{u}_c = \left\{w_1, -w_1', w_2, -w_2'\right\},$$

$$\mathbf{u}_d = \{\theta_{11}, \theta_{12}\} \tag{11}$$

where $\mathbf{N}_i$ ($i = b, c, d$) are shape functions, v_j and w_j (j = 1, 2) are nodal values of v and w at nodes j, respectively, v_j' and w_j' (j = 1, 2) are nodal values of $v_{,x}$ and $w_{,x}$at nodes j, respectively, and θ_{1j} ($j = 1, 2$) (j = 1, 2) are nodal values of θ_1 at nodes j, respectively.

The axial displacements of the shear center axis may be determined from the lateral deflections and the unit extension of the shear center axis using Eq. 9.

Ifx, $y$and z in Eq. 2 are regarded as the Lagrangian coordinates, the Green strain ε_{11},ε_{12} and $\varepsilon_{13}$are given by [Chung (1988)]

$$\varepsilon_{11} = \frac{1}{2}(\mathbf{r}_{,x}^t \mathbf{r}_{,x} - 1), \quad \varepsilon_{12} = \frac{1}{2}\mathbf{r}_{,x}^t \mathbf{r}_{,y}, \quad \varepsilon_{13} = \frac{1}{2}\mathbf{r}_{,x}^t \mathbf{r}_{,z}. \tag{12}$$

2.5 Nodal parameters and forces

The element employed here has two nodes with six degrees of freedom per node. Two sets of element nodal parameters termed 'explicit nodal parameters' and 'implicit nodal parameters' are employed. The explicit nodal parameters of the element are used for the assembly of the system equations from the element equations. They are chosen to be u_{ij} ($u_{1j} = u_j$, $u_{2j} = v_j$, $u_{3j} = w_j$) and ϕ_{ij}, the x_i (i = 1, 2, 3) components of the translation vectors $\mathbf{u}_j$ and the x_i components of the rotation vectors ϕ_j at node j (j = 1, 2), respectively. Here, the values of ϕ_j are reset to zero at current configuration. The generalized nodal forces corresponding to δu_{ij} and $\delta\phi_{ij}$ are f_{ij}, and m_{ij}, the forces in the x_i directions and the conventional moments about the x_i axes, respectively.

The implicit nodal parameters of the element are used to determine the deformation of the beam element. They are chosen to be u_{ij}, and θ_{ij}^* $\left(\theta_{1j}^* = \theta_{1j},\ \theta_{2j}^* = -w_j',\ \theta_{3j}^* = v_j'\right)$, at node j. The generalized nodal forces corresponding to δu_{ij} and $\delta\theta_{ij}^*$ are f_{ij} and m_{ij}^θ, the forces in the x_i directions, and the generalized moments, respectively. Note that m_{ij}^θ are not conventional moments, because $\delta\theta_{ij}^*$ are not infinitesimal rotations about the x_i axes at deformed state.

The relations between the variation of the implicit and explicit nodal parameters may be expressed as [Hsiao (1992]]

$$\delta\mathbf{q}_\theta=\begin{Bmatrix}\delta\mathbf{u}_1\\ \delta\boldsymbol{\theta}_1^*\\ \delta\mathbf{u}_2\\ \delta\boldsymbol{\theta}_1^*\end{Bmatrix}=\begin{bmatrix}\mathbf{I} & \mathbf{0} & \mathbf{0} & \mathbf{0}\\ \mathbf{T}_{b1} & \mathbf{T}_{a1} & -\mathbf{T}_{b1} & \mathbf{0}\\ \mathbf{0} & \mathbf{0} & \mathbf{I} & \mathbf{0}\\ \mathbf{T}_{b2} & \mathbf{0} & -\mathbf{T}_{b2} & \mathbf{T}_{a2}\end{bmatrix}=\begin{Bmatrix}\delta\mathbf{u}_1\\ \delta\boldsymbol{\phi}_1\\ \delta\mathbf{u}_2\\ \delta\boldsymbol{\phi}_2\end{Bmatrix}=\mathbf{T}_{\theta\phi}\delta\mathbf{q} \tag{13}$$

$$\mathbf{T}_{bj}=\begin{bmatrix}0 & 0 & 0\\ -\theta_{2j}/L & 0 & 0\\ -\theta_{3j}/L & 0 & 0\end{bmatrix},$$

$$\mathbf{T}_{aj}=\begin{bmatrix}1 & \theta_{3j}/2 & -\theta_{2j}/2\\ -\theta_{3j} & 1+\varepsilon_c & 0\\ \theta_{2j} & 0 & 1+\varepsilon_c\end{bmatrix},\ (j=1,2) \tag{14}$$

where $\delta\mathbf{u}_j=\{\delta u_j,\delta v_j,\delta w_j\}$, $\delta\boldsymbol{\theta}_j^*=\{\delta\theta_{1j},-\delta w_j',\delta v_j'\}$, and $\delta\boldsymbol{\phi}_j=\{\delta\phi_{1j},\delta\phi_{2j},\delta\phi_{3j}\}$ (j = 1, 2); $\mathbf{I}$ and $\mathbf{0}$ are the identity and zero matrices of order 3×3.

The global nodal parameters for the structural system corresponding to the element local nodes j (j = 1, 2) should be consistent with the element explicit nodal parameters. Thus, they are chosen to be the X_i^G components of the translation vectors and the X_i^G components of the rotation vectors at nodes j. Here, the values of nodal rotation vectors are reset to zero at current configuration. The corresponding generalized nodal forces are forces in the X_i^G directions and conventional moments about the X_i^G axes, respectively.

2.6 Element nodal force vector

The implicit element nodal forces are obtained from the virtual work principle in the current element coordinates. For convenience, the implicit nodal parameters are divided into four generalized nodal displacement vectors $\mathbf{u}_i$ ($i=a, b, c, d$), where

$$\mathbf{u}_a=\{u_1,u_2\} \tag{15}$$

and $\mathbf{u}_b$, $\mathbf{u}_c$, and $\mathbf{u}_d$ are defined in Eq. 11.

The generalized force vectors corresponding to $\delta\mathbf{u}_i$, the variation of $\mathbf{u}_i$ ($i=a, b, c, d$), are

$$\begin{aligned}&\mathbf{f}_a=\{f_{11},f_{12}\},\quad \mathbf{f}_b=\{f_{21},m_{31}^\theta,f_{22},m_{32}^\theta\}\\ &\mathbf{f}_c=\{f_{31},m_{21}^\theta,f_{32},m_{22}^\theta\},\quad \mathbf{f}_d=\{m_{11}^\theta,m_{12}^\theta\}.\end{aligned} \tag{16}$$

For linear elastic material, the virtual work principle requires that

$$\begin{aligned}&\delta\mathbf{u}_a^t\mathbf{f}_a+\delta\mathbf{u}_b^t\mathbf{f}_b+\delta\mathbf{u}_c^t\mathbf{f}_c+\delta\mathbf{u}_d^t\mathbf{f}_d\\ &=\int_V(E\varepsilon_{11}\delta\varepsilon_{11}+4G\varepsilon_{12}\delta\varepsilon_{12}+4G\varepsilon_{13}\delta\varepsilon_{13})dV\end{aligned} \tag{17}$$

where V is the volume of the undeformed beam, E is Young's modulus, G is the shear modulus, and $\delta\varepsilon_{1j}$ (j = 1, 2, 3) are the variation of ε_{1j} in Eq. 12 with respect to the implicit nodal parameter.

From Eqs. 12 and 17, retaining all the terms up to the second order of rotation parameters and their spatial derivatives, and retaining the third order terms of the twist rate, we may obtain

$$\begin{aligned}\mathbf{f}_a=&\Big[AEL\varepsilon_c(1+\frac{3}{2}\varepsilon_c)+\frac{1}{2}EI_p\int\theta_{1,x}^2dx\\ &+\frac{1}{2}EI_y\int w_{,xx}^2dx+\frac{1}{2}EI_z\int v_{,xx}^2dx\Big]\mathbf{G}_a\end{aligned} \tag{18}$$

$$\begin{aligned}\mathbf{f}_b=&EI_z(1+\varepsilon_c)\int\mathbf{N}''_b v_{,xx}dx+E(I_z-I_y)\int\mathbf{N}''_b\theta_1 w_{,xx}dx\\ &+f_{12}\mathbf{G}_b+\frac{1}{2}GJ\int(\mathbf{N}''_b\theta_{1,x}w_{,x}-\mathbf{N}'_b\theta_{1,x}w_{,xx})dx\end{aligned} \tag{19}$$

$$\begin{aligned}\mathbf{f}_c=&EI_y(1+\varepsilon_c)\int\mathbf{N}''_c w_{,xx}dx+E(I_z-I_y)\int\mathbf{N}''_c\theta_1 v_{,xx}dx\\ &+f_{12}\mathbf{G}_c+\frac{1}{2}GJ\int(\mathbf{N}'_c\theta_{1,x}v_{,xx}-\mathbf{N}''_c\theta_{1,x}v_{,x})dx\end{aligned} \tag{20}$$

$$\begin{aligned}\mathbf{f}_d=&[GJ+EI_p\varepsilon_c]\int\mathbf{N}'_d\theta_{1,x}dx+E(I_z-I_y)\int\mathbf{N}_d v_{,xx}w_{,xx}dx\\ &+\frac{1}{2}GJ\int\mathbf{N}'_d(w_{,x}v_{,xx}-v_{,x}w_{,xx})dx+\underline{\frac{1}{2}EK_I\int\mathbf{N}'_d\theta_{1,x}^3dx}\end{aligned} \tag{21}$$

where

$$\begin{aligned}&\mathbf{G}_a=\frac{1}{L}\{-1,1\},\quad \mathbf{G}_b=\int\mathbf{N}'_b v_{,x}dx,\quad \mathbf{G}_c=\int\mathbf{N}'_c w_{,x}dx\\ &I_y=\int z^2dA,\quad I_z=\int y^2dA,\quad K_I=\int(y^2+z^2)^2dA,\\ &I_p=I_y+I_z,\quad J=\int[(-z+\omega_{,y})^2+(y+\omega_{,z})^2]dA,\end{aligned} \tag{22}$$

in which the range of integration for the integral $\int(\ )dx$ in Eqs. 18-22 is from 0 to L, A is the cross section area, and $\mathbf{N}_j$ $(j=b,c,d)$ are given in Eq. 10. The underlined term in Eq. 21 is the third order term of $\theta_{1,x}$

Let $\mathbf{f}=\{\mathbf{f}_1,\mathbf{m}_1,\mathbf{f}_2,\mathbf{m}_2\}$, $\mathbf{f}_\theta=\{\mathbf{f}_1,\mathbf{m}_1^\theta,\mathbf{f}_2,\mathbf{m}_2^\theta\}$, where $\mathbf{f}_j=\{f_{1j},f_{2j},f_{3j}\}$, $\mathbf{m}_j=\{m_{1j},m_{2j},m_{3j}\}$, and $\mathbf{m}_j^\theta=\{m_{1j}^\theta,m_{2j}^\theta,m_{3j}^\theta\}$ (j = 1, 2), denote the internal nodal force vectors corresponding to the variation of the explicit and implicit nodal parameters, $\delta\mathbf{q}$ and $\delta\mathbf{q}_\theta$, respectively. Note that only the terms up to the second order of nodal parameters and the third order term of $\theta_{1,x}$ are retained in $\mathbf{f}_\theta$. Thus, using the contragradient law [Dawe (1984)] and Eq. 13, the corresponding $\mathbf{f}$ may be given by

$$\mathbf{f}=\mathbf{f}_\theta+(\mathbf{T}_{\theta\phi}^t-\mathbf{I}_{12})\mathbf{f}_\theta^1 \tag{23}$$

where $\mathbf{f}_\theta^1$ is the first order terms of nodal parameters of $\mathbf{f}_\theta$, and $\mathbf{I}_{12}$ is the identity matrix of order 12×12.

2.7 Element tangent stiffness matrices

The explicit element tangent stiffness matrix may be obtained by differentiating the element nodal force vector $\mathbf{f}$ in Eq. 23 with respect to explicit nodal parameters. Using Eqs. 13 and 23, we obtain

$$\mathbf{k}=\frac{\partial\mathbf{f}}{\partial\mathbf{q}}=\frac{\partial\mathbf{f}}{\partial\mathbf{q}_\theta}\frac{\partial\mathbf{q}_\theta}{\partial\mathbf{q}}=[\mathbf{k}_\theta+(\mathbf{T}_{\theta\phi}^t-\mathbf{I}_{12})\mathbf{k}_\theta^0+\mathbf{H}]\mathbf{T}_{\theta\phi} \tag{24}$$

where $\mathbf{k}_\theta=\partial\mathbf{f}_\theta/\partial\mathbf{q}_\theta$ is the implicit element tangent stiffness matrix, $\mathbf{k}_\theta^0$ is the zeroth order terms of nodal parameters of $\mathbf{k}_\theta$, and $\mathbf{H}$ is a unsymmetrical matrix and is given by

$$\mathbf{H}=\begin{bmatrix}\mathbf{0}&\mathbf{h}_{b1}&\mathbf{0}&\mathbf{h}_{b2}\\ \mathbf{h}_{b1}^t&\mathbf{h}_{a1}&-\mathbf{h}_{b1}^t&\mathbf{0}\\ \mathbf{0}&-\mathbf{h}_{b1}&\mathbf{0}&-\mathbf{h}_{b2}\\ \mathbf{h}_{b2}^t&\mathbf{0}&-\mathbf{h}_{b2}^t&\mathbf{h}_{a2}\end{bmatrix} \tag{25}$$

$$\mathbf{h}_{bj}=\begin{bmatrix}0&-\frac{m_{2j}^{\theta1}}{L}&-\frac{m_{2j}^{\theta1}}{L}\\ 0&0&0\\ 0&0&0\end{bmatrix},\ \mathbf{h}_{aj}=\begin{bmatrix}0&m_{3j}^{\theta1}&-m_{2j}^{\theta1}\\ 0&0&\frac{1}{2}m_{1j}^{\theta1}\\ 0&-\frac{1}{2}m_{1j}^{\theta1}&0\end{bmatrix},\quad(j=1,2) \tag{26}$$

where $\mathbf{0}$ and is zero matrix of order 3×3, $m_{ij}^{\theta1}$ (i = 1, 2, 3, j = 1, 2) are the first order terms of m_{ij}^θ.

Using the direct stiffness method, the implicit tangent stiffness matrix $\mathbf{k}_\theta$ may be assembled by the submatrices

$$\mathbf{k}_{ij}=\frac{\partial\mathbf{f}_i}{\partial\mathbf{u}_j} \tag{27}$$

where $\mathbf{f}_i$ $(i=a,\ b,\ c,\ d)$ are defined in Eqs. 18-21 and $\mathbf{u}_i$ $(i=a,\ b,\ c,\ d)$ are defined in Eqs. 11 and 15. Note that $\mathbf{k}_{ij}$ are symmetric matrices. The explicit form of $\mathbf{k}_{ij}$ may be expressed as

$$\begin{aligned}
\mathbf{k}_{aa}&=AEL(1+3\varepsilon_c)\mathbf{G}_a\mathbf{G}_a^t,\\
\mathbf{k}_{ab}&=\mathbf{G}_a(AE\mathbf{G}_b^t+EI_z\int\mathbf{N}''^t_b v_{,xx}dx)\\
\mathbf{k}_{ac}&=\mathbf{G}_a(AE\mathbf{G}_c^t+EI_y\int\mathbf{N}''^t_c w_{,xx}dx),\\
\mathbf{k}_{ad}&=EI_p\mathbf{G}_a\int\mathbf{N}'^t_d\theta_{1,x}dx\\
\mathbf{k}_{bb}&=EI_z(1+\varepsilon_c)\int\mathbf{N}''_b\mathbf{N}''^t_b dx+f_{12}\int\mathbf{N}'_b\mathbf{N}'^t_b dx\\
\mathbf{k}_{bc}&=E(I_z-I_y)\int\mathbf{N}''_b\mathbf{N}''^t_c\theta_1 dx\\
&\quad+\frac{1}{2}GJ\int(\mathbf{N}''_b\mathbf{N}'^t_c-\mathbf{N}'_b\mathbf{N}''^t_c)\theta_{1,x}dx\\
\mathbf{k}_{bd}&=E(I_z-I_y)\int\mathbf{N}''_b\mathbf{N}^t_d w_{,xx}dx\\
&\quad+\frac{1}{2}GJ\int(\mathbf{N}''_b\mathbf{N}'^t_d w_{,x}-\mathbf{N}'_b\mathbf{N}'^t_d w_{,xx})dx\\
\mathbf{k}_{cc}&=EI_y(1+\varepsilon_c)\int\mathbf{N}''_c\mathbf{N}''^t_c dx+f_{12}\int\mathbf{N}'_c\mathbf{N}'^t_c dx\\
\mathbf{k}_{cd}&=E(I_z-I_y)\int\mathbf{N}''_c\mathbf{N}^t_d v_{,xx}dx\\
&\quad+\frac{1}{2}GJ\int(\mathbf{N}'_c\mathbf{N}'^t_d v_{,xx}-\mathbf{N}''_c\mathbf{N}'^t_d v_{,x})dx\\
\mathbf{k}_{dd}&=[GJ+EI_p\varepsilon_c]\int\mathbf{N}'_d\mathbf{N}'^t_d dx+\underline{\frac{3}{2}EK_I\int\mathbf{N}'_d\mathbf{N}'^t_d\theta_{1,x}^2dx},
\end{aligned} \tag{28}$$

where the underlined term is the second order term of $\theta_{1,x}$.

2.8 Load stiffness matrix

Different ways for generating configuration dependent moment were proposed in the literature [Ziegler (1977); Argyris, Dunne, and Scharpf (1978); Iura and Atluri (1988); Teh and Clarke (1997); Hsiao, Yang and Lin

(1998)]. Here, the ways for generating conservative moment proposed in [Hsiao, Yang and Lin (1998)] are employed. For completeness, a brief description of the ways for generating conservative moment is given here. In this study, a set of load base coordinates X_i^P (i = 1, 2, 3) associated with each configuration dependent moment is constructed at the current configuration to describe the mechanism for generating configuration dependent moment. The way for generating configuration dependent moment may be described as follows.

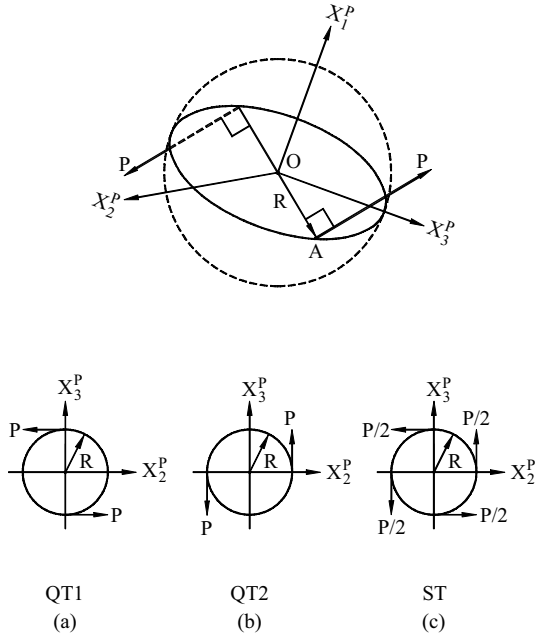

Figure 3 : Mechanism for generating configuration dependent moment.

Consider a sphere of radius R which centroid is rigidly connected with the structure at node O as shown in Fig. 3. Two strings wound around a great circle of the sphere are acted upon by forces of magnitude P. Thus, the strings are always tangent to the sphere. The great circle and the forces are on the same plane at the undeformed configuration of the structure. The origin of the load base coordinate system is chosen to be located at the node O. The X_1^P axis is chosen to coincide with the normal of the plane of the great circle, and the X_2^P and X_3^P axes lie in the plane of the great circle.

Three special cases shown in Fig. 3 are considered here. Following [Ziegler (1977)], they are referred to as quasitangential (QT) moments of the first and second type, and semitangential (ST) moment. The load stiffness matrices corresponding to QT and ST moment may given by [Hsiao, Yang and Lin (1998)]

$$\mathbf{k}_p^{QT1} = M\begin{bmatrix} 0 & 0 & 0 \\ 0 & 0 & 0 \\ 0 & -1 & 0 \end{bmatrix}, \quad \mathbf{k}_p^{QT2} = M\begin{bmatrix} 0 & 0 & 0 \\ 0 & 0 & 1 \\ 0 & 0 & 0 \end{bmatrix},$$
$$\mathbf{k}_p^{ST} = \frac{M}{2}\begin{bmatrix} 0 & 0 & 0 \\ 0 & 0 & 1 \\ 0 & -1 & 0 \end{bmatrix}. \tag{29}$$

where $M = 2RP$ is the magnitude of the moment.

2.9 Criterion of the buckling state

Here, the zero value of the tangent stiffness matrix determinant is used as the criterion of the buckling state. The tangent stiffness matrix of the structure is assembled from the element stiffness matrix and load stiffness matrix at the current equilibrium configuration. Let $\mathbf{K}_T(\lambda)$ denote the tangent stiffness matrix of the structure at the equilibrium configuration corresponding to the loading parameter λ. The criterion of the buckling state may be expressed as

$$D(\lambda) = \det|\mathbf{K}_T(\lambda)| = 0. \tag{30}$$

Let λ_{nb} denote the minimum loading parameter satisfying Eq. 30. λ_{nb} is called buckling loading parameter here.

3 Numerical algorithm

An incremental-iterative method based on the Newton-Raphson method combined with constant arc length of incremental displacement vector [Hsiao (1992); Crisfield (1981)] is employed for the solution of nonlinear equilibrium equations. For a given displacement increment or corrector, the method described in [Hsiao and Tsay (1991)] is employed to determine the current element cross section coordinates, element coordinates and element deformation nodal parameters for each element. A bisection method of the arc length is employed here to find the buckling load. In order to initiate the secondary path, at the bifurcation point a perturbation displacement proportional to the first buckling mode is added [Matsui and Matsuoka (1976)].

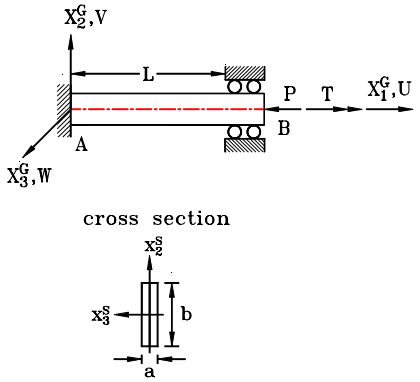

Figure 4 : Rod subjected to end torque and axial force.

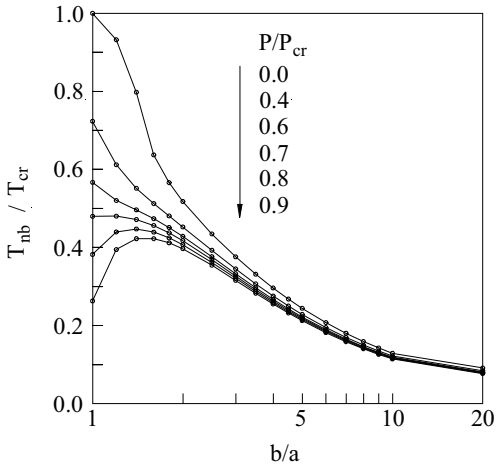

Figure 5 : Buckling torque versus aspect ratio of cross section for the first example

4 Numerical studies

The Young's modulus $E = 2 \times 10^7\ N/cm^2$ and shear modulus $G = 7.9 \times 10^6\ N/cm^2$ are used here.

In order to verify the present method, the first example considered is the example given in [Goto, Li, and Kasugal (1996)] as shown in Fig. 4. The geometry properties are: $L = 720\ cm$, and $a = 1\ cm$. The classical linear buckling torque for pure torsion is $T_{cr} = \frac{2.861\pi E}{L}\sqrt{I_y I_z}$ [Goto, Li, and Kasugal (1996)]. The classical linear buckling force for pure compressive axial force is $P_{cr} = \frac{4\pi^2 E I_y}{L^2}$ [Timoshenko and Gere (1963)].

The results of the present study are obtained by using 160 elements and shown in Table 1 and Fig. 5. A plot of nondimensional buckling torque T_{nb}/T_{cr} versus $\log(b/a)$ for various values of P/P_{cr} is shown in Fig. 5. The present results given in Fig. 5 and those reported by [Goto, Li, and Kasugal (1996)] (for $b/a \leq 10$, not shown here) are nearly identical.

Table 1 : Buckling moment for example 1

$\frac{b}{a} \backslash \frac{P}{P_{cr}}$	T_{nb}/T_{cr}				
	0.0	0.4	0.6	0.8	0.9
1.0	0.9998	0.7223	0.5666	0.3819	0.2629
1.2	0.9320	0.6119	0.5203	0.4397	0.3947
1.6	0.6370	0.5124	0.4737	0.4392	0.4224
2.0	0.5177	0.4525	0.4284	0.4069	0.3967
5.0	0.2441	0.2284	0.2218	0.2156	0.2126
10.0	0.1290	0.1218	0.1187	0.1157	0.1143
20.0	0.0913	0.0843	0.0812	0.0783	0.0770

The load-end axial displacement curves in the secondary equilibrium paths for different cases are shown in Figs. 6-8. As can be seen from Fig. 6, the agreement between the present results and those given in [Goto, Li, and Kasugal (1996)] is very good. Numerical experiment has shown that when $b/a \leq 10$, the effect of the third order term of the twist rate is negligible for the buckling analysis.

The second example considered is a cantilever rod subjected to end torque T as shown in Fig. 9. The QT2 torque is considered. The geometry properties are: L = 400 cm, $a = 1$ cm, and b = 20 cm. The classical linear buckling torque for pure torsion is quoted in [Yang and Kuo (1991)] as $T_{cr} = \frac{\pi E}{2L}\sqrt{I_y I_z} = 2.618 \times 10^4\ kN \cdot cm$. The classical linear buckling force for pure axial compressive force is $P_{cr} = \frac{\pi^2 E I_y}{4L^2}$ [Timoshenko and Gere (1963)].

In order to investigate the effect of third order term of the twist rate on the buckling torque of three-dimensional rods, the following cases are considered:

1. TR = 1 – All the terms in Eq. 21, and Eq. 28 are considered.

2. TR = 2 – Except the term $EI_p\varepsilon_c \int \mathbf{N}_d' \theta_{1,s} ds$ and $\frac{1}{2}EK_I \int \mathbf{N}_d' \theta_{1,s}^3 ds$ in Eq. 21, all the terms in Eq. 21, and the corresponding terms in Eq. 28 are considered.

3. TR = 3 – Except the term $\frac{1}{2}EK_I \int \mathbf{N}_d' \theta_{1,s}^3 ds$ in Eq. 21 all the terms in Eq. 21 and the corresponding terms in Eq. 28 are considered.

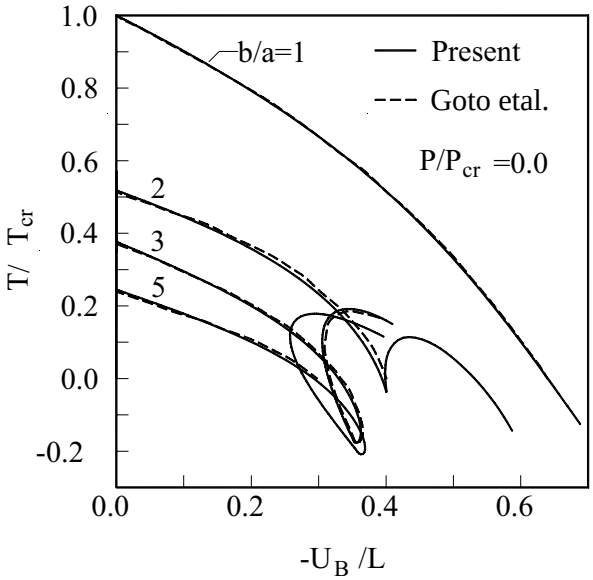

Figure 6 : Load-end axial displacement for the first example

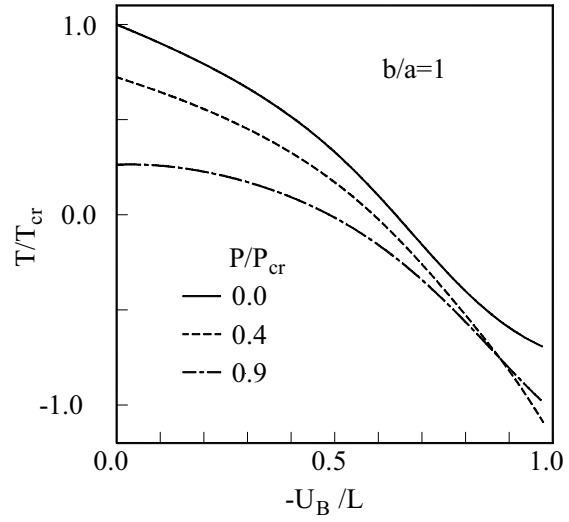

Figure 7 : Load-end axial displacement for the first example

It is observed that the only nonzero deformations are uniform twist rate $\theta_{1,s}$ and uniform unit extension of the centroid axis ε_c for this example. From Eq. 18, and using the approximation $1+\frac{3}{2}\varepsilon_c \approx 1$, one may obtain $\varepsilon_c = -\frac{I_p}{2A}\theta_{1,s}^2 - \frac{P}{AE}$. As can be seen that ε_c is a second order term of twist rate. Thus, $EI_p\varepsilon_c \int \mathbf{N}_d'\theta_{1,s}ds$ in Eq. 21 may be regarded as a third order term of $\theta_{1,s}$.

It is seen that the twist moment-twist rate relation is linear for TR = 2, and nonlinear twist moment-twist rate relations are used for TR = 1, 3. However, the third order term for TR = 3 is incomplete. Thus the results corresponding to TR = 3 may not be reliable for the buckling torque of three-dimensional rods with very narrow rectangular cross section.

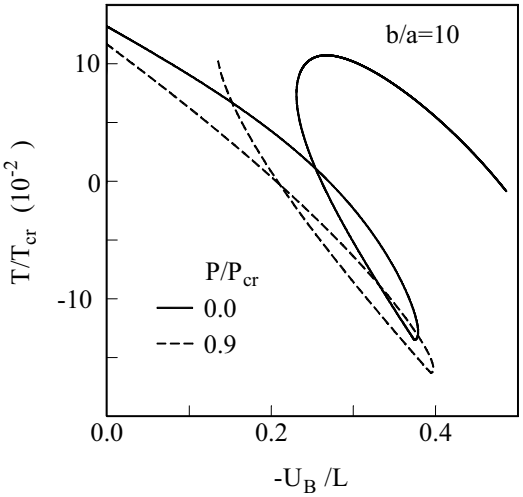

Figure 8 : Load-end axial displacement for the first example

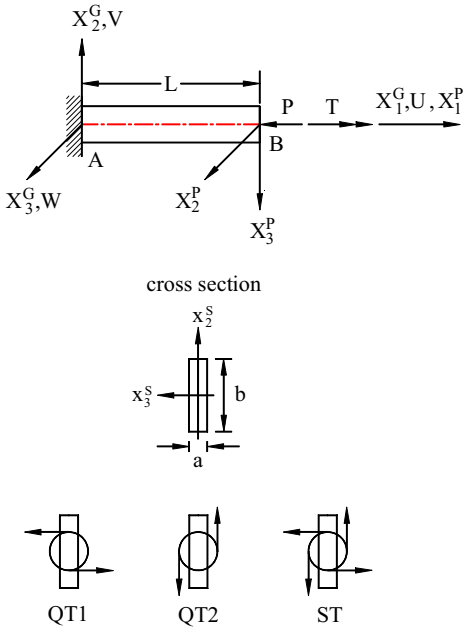

Figure 9 : Cantilever rod subjected to end torque and axial force.

The buckling torques for different cases are given in Tab.

Table 2 : Buckling moment for example 2

P/P_{cr}	Number of elements	$T_{nb}(10^3 kN \cdot cm)$		
		TR = 1	TR = 2	TR = 3
0	80	3.518	3.142	2.642
	120	3.535	3.155	2.650
	160	3.541	3.160	2.652
	200	3.543	3.162	2.653
0.9	80	3.337	2.971	2.517
	120	3.351	2.982	2.524
	160	3.356	2.986	2.527
	200	3.359	2.988	2.528

2. As can be seen, the discrepancy among the buckling moments corresponding to TR = 1-3 is not negligible, and the discrepancy between the present buckling moments and the classical linear buckling moments are remarked. From this example, it shows clearly that the third order term of the twist rate in the element nodal forces and the corresponding term in the element stiffness matrix are not negligible for the buckling torque of three dimensional rods with very narrow rectangular cross section. As can be seen that a large number of elements are required for the convergence of the buckling moment. The large aspect ratio of the cross section and the assumption of uniform twist rate may be one of the reasons for this slow convergence.

The third example is a cantilever rod subjected to end torque T as shown in Fig. 9. The quasitangential and semitangential torques are considered. The geometry properties are identical with those of the first example. The classical linear buckling torque for pure torsion is quoted in [Yang and Kuo (1991)] as $T_{cr} = \frac{\pi E}{2L}\sqrt{I_y I_z}$ for QT and $T_{cr} = \frac{\pi E}{L}\sqrt{I_y I_z}$ for ST.

The classical linear buckling force for pure compressive axial force is $P_{cr} = \frac{\pi^2 E I_y}{4L^2}$ [Timoshenko and Gere (1963)]. The results of the present study are obtained by using 160 elements. The nondimensional buckling torques T_{nb}/T_{cr} for different cases are given in Tables 3-5 and Fig. 10-12. Figures 10-12 are plots of nondimensional buckling torque T_{nb}/T_{cr} versus log (b/a) for different types of torque. It can be seen that the values of T_{nb}/T_{cr} are much influenced by the aspect ratio b/a and decrease with the increase of the compressive axial force. For the case of QT2 torque the value of T_{nb}/T_{cr} increases and then decreases with the increase of b/a, and $T_{nb}/T_{cr} \geq 1$ when $b/a \leq 1.6$. However, for the case of ST torque the value of T_{nb}/T_{cr} monotonically decreases with the increase of b/a. It is interesting to note that the buckling torques for the rod with large aspect ratio (say $b/a \geq 5$) are much smaller than the linear buckling torques for various types of torques. The load-deflection curves in the secondary equilibrium paths for the case of b/a = 1 and 20 are shown in Figs. 13-15 and 16-18, respectively.

Table 3 : Buckling moment for example 3 (QT1)

$\frac{b}{a}\backslash\frac{P}{P_{cr}}$	T_{nb}/T_{cr}(QT1)				
	0.0	0.4	0.6	0.8	0.9
1.0	1.0000	0.6808	0.4923	0.2727	0.1453
1.2	0.8502	0.5739	0.4367	0.2831	0.1893
1.6	0.6253	0.4483	0.3568	0.2473	0.1733
2.0	0.5017	0.3722	0.3016	0.2138	0.1520
5.0	0.2106	0.1646	0.1370	0.1002	0.0727
10.0	0.1075	0.0849	0.0710	0.0523	0.0380
20.0	0.0545	0.0432	0.0361	0.0226	0.0194

Table 4 : Buckling moment for example 3 (QT2)

$\frac{b}{a}\backslash\frac{P}{P_{cr}}$	T_{nb}/T_{cr}(QT2)				
	0.0	0.4	0.6	0.8	0.9
1.0	1.0000	0.6808	0.4923	0.2727	0.1453
1.2	1.0633	0.8948	0.7810	0.6139	0.4749
1.6	1.0039	0.9420	0.9092	0.8743	0.8558
2.0	0.8979	0.8598	0.8400	0.8192	0.8082
5.0	0.4450	0.4336	0.4274	0.4206	0.4169
10.0	0.2356	0.2302	0.2272	0.2239	0.2221
20.0	0.1253	0.1225	0.1210	0.1194	0.1185

Table 5 : Buckling moment for example 3 (ST)

$\frac{b}{a}\backslash\frac{P}{P_{cr}}$	T_{nb}/T_{cr}(ST)				
	0.0	0.4	0.6	0.8	0.9
1.0	1.0000	0.7745	0.6324	0.4472	0.3162
1.2	0.8502	0.6483	0.5282	0.3759	0.2682
1.6	0.6253	0.4862	0.4014	0.2906	0.2096
2.0	0.5017	0.3951	0.3285	0.2997	0.1738
5.0	0.2105	0.1690	0.1420	0.1050	0.0768
10.0	0.1074	0.0866	0.0729	0.0540	0.0396
20.0	0.0559	0.0446	0.0374	0.0275	0.0201

5 Conclusions

The buckling and postbuckling behavior of spatial rods under different types of end torque and compressive axial force is investigated using finite element method.

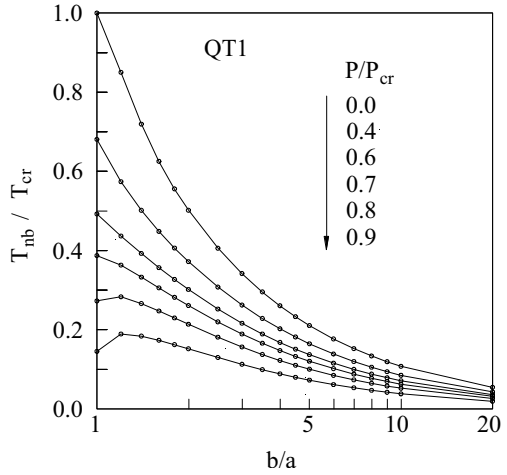

Figure 10 : Buckling torque (QT1) versus aspect ratio of cross section for cantilever rod.

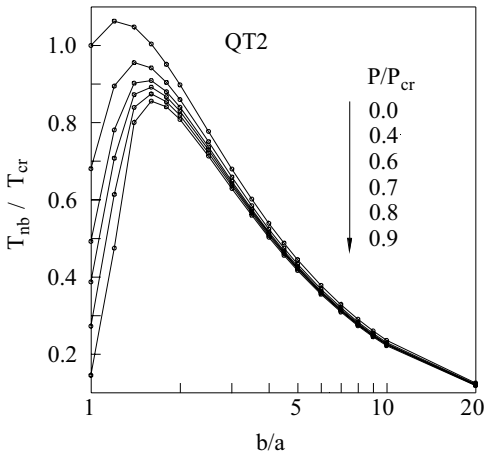

Figure 11 : Buckling torque (QT2) versus aspect ratio of cross section for cantilever rod.

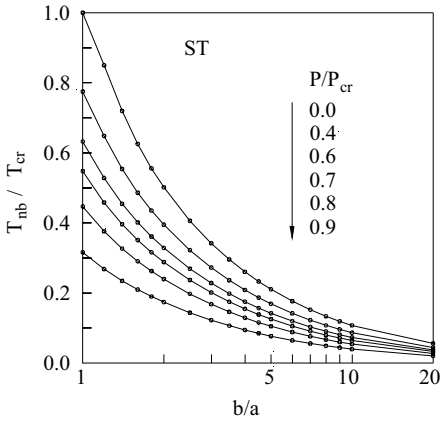

Figure 12 : Buckling torque (ST) versus aspect ratio of cross section for cantilever rod.

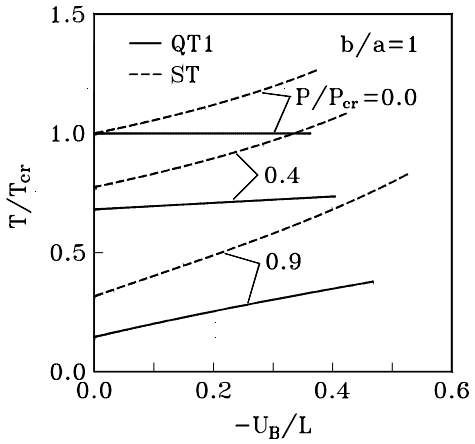

Figure 13 : Load-tip displacement for cantilever rod

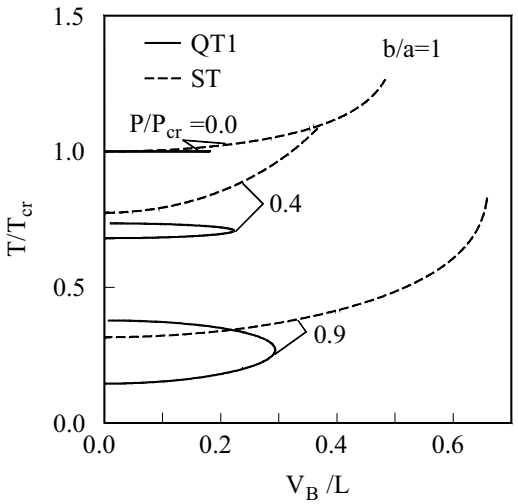

Figure 14 : Load-tip displacement for cantilever rod

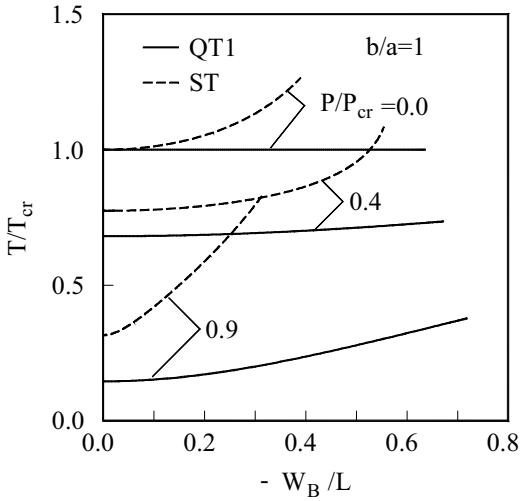

Figure 15 : Load-tip displacement for cantilever rod

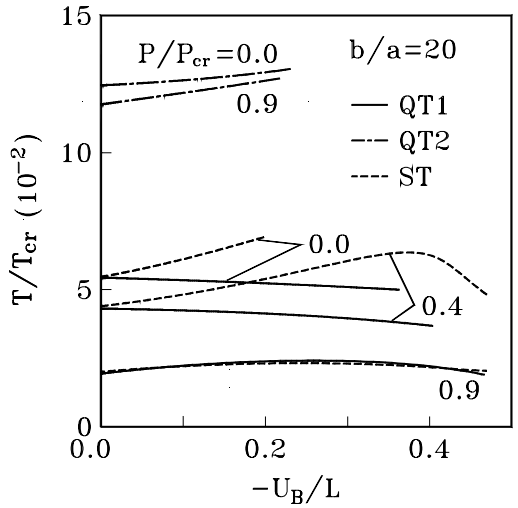

Figure 16 : Load-tip displacement for cantilever rod

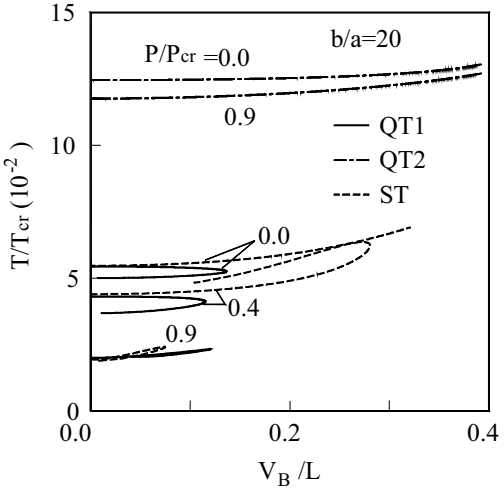

Figure 17 : Load-tip displacement for cantilever rod

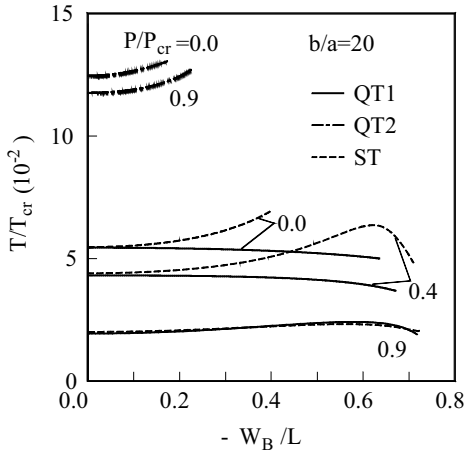

Figure 18 : Load-tip displacement for cantilever rod

The consistent co-rotational finite element formulation for three-dimensional Euler beam presented by Hsiao and Lin (2000) is employed here. All coupling among bending, twisting, and stretching deformations for beam element is considered by consistent second-order linearization of the fully geometrically nonlinear beam theory. However, the third order term of the twist rate is retained in the element nodal forces. From the numerical examples studied, it is found that the third order term of the twist rate in the element nodal forces and the corresponding term in the element stiffness matrix are not negligible for the buckling torque of three-dimensional beams with very narrow rectangular cross section. The buckling torques and postbuckling behaviors for a rod subjected to different types of torques are in general different. The buckling torques decrease with the increase of the compressive axial force. For the case of pure torsion, the buckling torques for the beam with square cross section exactly coincide with the linear buckling torques for various types of torques. However, the buckling torques for the rod with large aspect ratio is much smaller than the linear buckling torques for various types of torques.

Acknowledgement: The authors would like to acknowledge the constructive and thoughtful comments of the referee. The research was sponsored by the national Science Council, Taiwan (ROC) under the contract NSC 89-2212-E-009-052.

References:

Argyris J.H.; Dunne P.C.; Scharpf D.W. (1978): On large displacement-small strain analysis of structures with rotation degree of freedom. *Comput. Meth. Appl. Mech. Engng.*, vol. 14, pp. 401-451, vol. 15, pp. 99-135.

Atluri, S.N., Iura, M. and Vasudevan, S. (2001): A Consistent Theory of Finite Stretches and Finite Rotations, in Space-Curved Beams of Arbitrary Cross-Section, *Computational Mechanics*, vol. 27, pp. 271-281.

Attard M.M. (1986): Lateral buckling analysis of beams by FEM. *Comput. Struct.*, vol. 23, pp. 217-231.

Beck M. (1955): Knickung gerader stabe unter druck und konservativer torsion. *Ing. Arch.*, vol. 23, pp. 231-253.

Brush D.O.; Almroth B.O. (1975): *Buckling of Bars,*

Plates and shells. McGraw-Hill, New York.

Chung T.J. (1988); *Continuum Mechanics*. Prentice-Hall Englewood Cliffs, NJ.

Crisfield M.A. (1981): A fast incremental/iterative solution procedure that handles 'snap through'. *Comput. Struct.*, vol. 13, pp. 55-62.

Crisfield M.A. (1990): A consistent co-rotational formulation for non-linear, three-dimensional, beam elements. *Comput. Meth. Appl. Mech. Engng*., vol. 81, pp. 131-150.

Dawe D.J. (1984): *Matrix and Finite Element Displacement Analysis of Structures*. Oxford University Press, New York.

Goldstein H. (1980): *Classical Mechanics*. Addision-Wesley, Reading, MA.

Goto Y.; Li X.S.; Kasugal T. (1996): Buckling analysis of elastic space rods under torsional moment. *J. Engng. Mech. ASCE,* vol. **122**, pp. 826-833.

Greenhill A. G. (1883): On the strength of shafting when exposed both to torsion and to end thrust. *Proc. Inst. Mech. Engrs.*, pp. 182-225.

Gregory M. (1960): A nonlinear bending effect when certain unsymmetical sections are subjected to a pure torque, *Australian J. Appl. Sci*., vol. 11**,** pp. 33-48.

Hsiao K.M.; Tsay C.M. (1991): A motion process for large displacement analysis of spatial frames. *Int. J. space struct*., vol. 6, pp. 133-139.

Hsiao K.M. (1992): Corotational total Lagrangian formulation for three-dimensional beam element. *AIAA J*., vol. 30, pp. 797-804.

Hsiao K.M.; Yang R.T.; Lin W.Y. (1998): A consistent finite element formulation for linear buckling analysis of spatial beams. *Comput. Meth. Appl. Mech. Engn.*, vol. 156, pp. 259-276.

Hsiao K.M.; Lin W.Y. (2000): A co-rotational finite element formulation for buckling and postbuckling analysis of spatial beams. *Comput. Meth. Appl. Mech. Engng*., vol. 188, pp. 567-594.

Ijima K.; Obiya H.; Iguchi S.; Goto S. (to appear): Element coordinates and its utility in large displacement analysis of space frame. *CMES: Computer Modeling in Engineering and Sciences*, vol. 4, No. 2.

Iura M.; Atluri S. N. (1988): Dynamic analysis of finitely stretched and rotated three-dimensional space-curved beams. *Comput. Struct*., vol. 29, pp. 875-889.

Izzuddin B.A.; Smith D.L. (1996): Large-displacement analysis of elastoplastic thin-walled frames, part I: formulation and implementation and part II: verification and application. *J. Struct. Engrg. ASCE,* vol. 122 905-925.

Matsui T.; Matsuoka O. (1976): A new finite element scheme for instability analysis of thin shells. *Int. J. Numer. Meth. Engng.*, vol. 10, pp. 145-170.

Simo J.C.; Vu-Quoc L. (1986): A three-dimensional finite strain rod model. Part II: Computational aspects. *Comput. Meth. Appl. Mech. Engng.*, vol. 58, pp. 79-116.

Teh L.H.; Clarke M.J. (1997): New definition of conservative internal moments in space frames. *J. Engng. Mech. ASCE,* vol. 123, pp. 97-106.

Teh L.H.; Clarke M.J. (1998): Co-rotational and Lagrangian formulations for elastic three-dimensional beam finite elements. *J. Construct. Steel Research*, vol. 48, pp. 123-144.

Timoshenko S. (1956): *Strength of Materials, Part II: Advanced Theory and Problems*. D. Van Nostrand Co., Inc. N.J..

Timoshenko S.P.; Gere J.M. (1963): Theory of Elastic Stability. McGraw-Hill, New York.

Yang Y.B.; Kuo S.R. (1991): Buckling of frames under various torsional loading. *J. Engng. Mech. ASCE,* vol. 117, pp. 1681-1697.

Ziegler H. (1952): Knickung gerader stabe unter torsion. *Z. Angew. Math. Phys*., vol. 3, pp. 96-119.

Ziegler H. (1977): *Principles of Structural Stability*. Birkhauser Verlag Basel.